Proceeding of International Conference on Electrical Engineering, Computer Science and Informatics (EECSI 2015), Palembang, Indonesia, 19 -20 August 2015

MDM of Hybrid Modes in Multimode Fiber

Angela Amphawan, Yousef Fazea, Mohd Samsu Sajat
School of Computing, Universiti Utara Malaysia,
Sintok, Kedah, Malaysia.
angela.amphawan.dr@ieee.org

Roslinda Murad, Hajar Alias
Department of Computer Science,
Kolej Poly-Tech MARA,
Cheras, Kuala Lumpur, Malaysia

***Abstract*—This paper reports on MDM of a combination of helical-phased modes comprising ring modes and HG modes. 44Gbps data transmission is achieved by a wavelength division multiplexing (WDM) - MDM system of two center-launched helical-phased ring modes and two 3μm radially offset HG mode on wavelengths 1550.12nm and 1551.72nm for a 1500m-long multimode fiber. The power coupling coefficients, degenerate mode group delays and bit error rates are analyzed for different HG modes and radial offsets.**

Keywords—Mode division multiplexing; spiral phase front; ring mode; Hermite-Gaussian modes; HG modes; vortex lens; multimode fiber; big data; cloud computing; optical communications

Introduction

Cloud computing trends from interactive multimedia services are thrusting changes towards enhancing scalability, agility, and reliability of data centers and access networks. Multimedia applications such as voice-over-internet-protocols (VoIP), television streaming, and security surveillance are flooding optical backbones, predominantly multimode fiber (MMF) [1]. In the quest to future proof data centers, it is imperative to tap into new multiplexing technologies as the surge of network traffic will soon overwhelm the capacity of MMF backbones in data centers and access networks [2, 3].

Mode division multiplexing (MDM) is a remarkable bandwidth enhancement technique whereby information is transmitted via propagating modes in MMF. This emerging technology exploits modal dispersion and offers another dimension for multiplexing several data channels in data centers through a single optical fiber in addition to wavelength, polarization, and time. In MDM, single or groups of modes are used to transmit disparate data streams in MMF by precise engineering of the launch field to optimize the differential mode delay and power coupling coefficients. Only a subset of selected modes are excited by matching the incident wave front at the input facet to the intrinsic fiber mode profile. MDM is realized by various mechanisms such as spatial light modulators [4-7] optical signal processing [8-10], few mode fiber [11-16], photonic crystal fibers [17] and modal decomposition methods [18-20].

Beams with helical phase fronts have attracted significant attention as data carriers in MMF [21].OAM modes have helical phase fronts with azimuthal phase variations corresponding to the OAM mode order and a ring-shaped intensity profile with a null in intensity at the center [22]. MDM of OAM modes have been demonstrated using spatial light modulators, equalizers and specially designed optical fiber [21, 23-25]. Apart from harnessing the capacity of MMF by providing additional data channels, ring-shaped OAM beams also circumvents central core regions where refractive index imperfections in manufactured MMF are most prevalent [26].

In this paper, MDM of a new combination of helical-phased modes comprising ring modes and radially offset Hermite-Gaussian (HG) modes is modeled using a vertical-cavity surface-emitting laser (VCSEL) array and a vortex lens and coupled into a MMF. The spatial electric fields, mode group delays and power-coupling coefficients into individual modes and degenerate mode groups are analyzed for various HG mode indices.

This paper proceeds as follows. Section II reports on the modeling of a new MDM scheme for helical-phased ring modes and radially offset HG modes. Section III analyzes the power coupling coefficients, degenerate mode group delays, and bit error rates for different HG modes. The paper is concluded in Section IV.

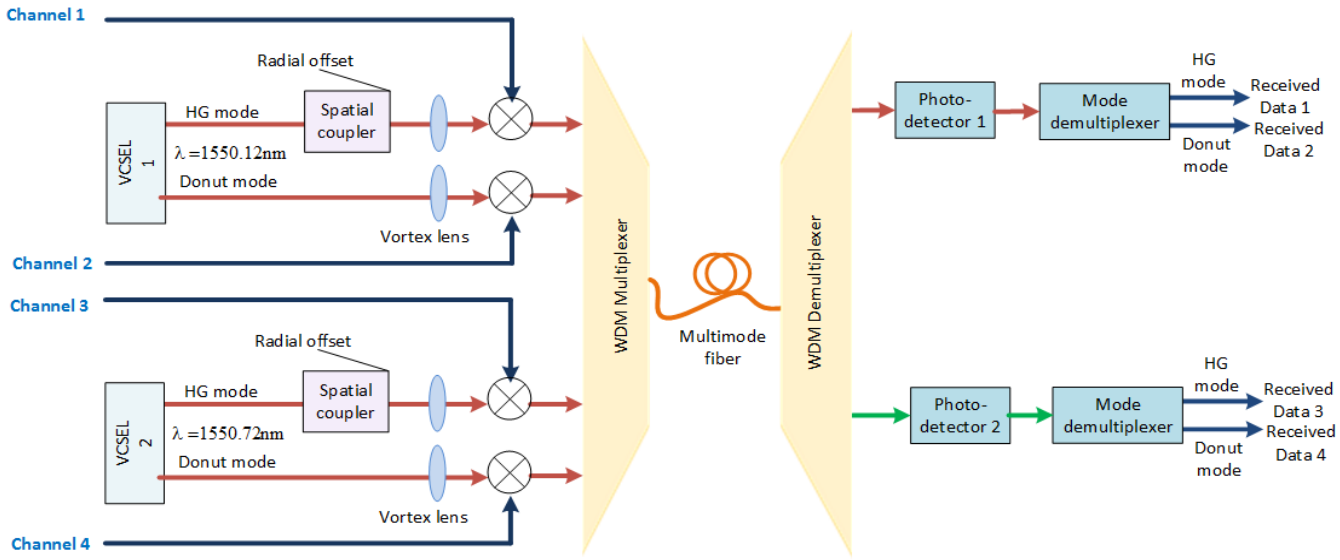

Fig. 1 MDM model for helical-phased ring modes and HG modes on two wavelengths

Simulation of spiral-phased ring Modes

MDM of helical-phased ring modes and HG modes in MMF was modeled in Optsim 5.2 [27] and Matlab, as shown in Fig. 1. The model may be divided into three parts, namely the transmitter, multimode fiber, and receiver.

The transmitter constitutes two VCSEL on 1550.12nm and 1551.72nm and four vortex lenses. Each VCSEL has an array emitting *x*-polarized ring modes with inner and outer radii of 10μm and 12µm respectively and a radially offset HG mode. The VCSEL is driven by pseudo-random binary sequence (PRBS) electrical signals and modulated to non-return-to-zero (NRZ) pulses. The generated transverse electrical field profile of the ring mode from the VCSEL array is described as [27]:

$$\psi(r,\phi)=\begin{cases}\kappa, & r_{\min}\le r\le r_{\max}\\ 0 & r>r_{\max}\end{cases} \quad (1)$$

where κ is normalization constant, r_{min} is the minimum radius, and r_{max} is the maximum radius of the ring. Within the minimum and maximum radii, the electric field is constant whereas outside of these bounds, the transverse electric field is zero. By driving a VCSEL at low current, HG modes may be generated [28]. The generated HG mode radially offset from the MMF core center is given by:

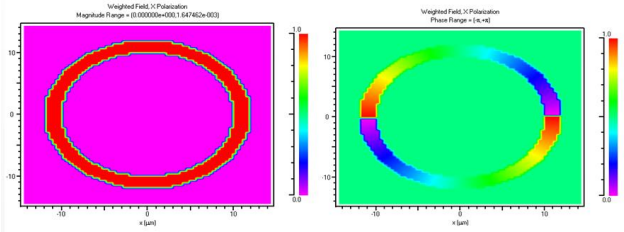

Fig. 2 Magnitude distribution (left) and phase distribution (right) of transverse electric field of ring mode from VCSEL array after vortex lens

from the MMF core center is given by:

$$\psi_{lm}(x,y)=\alpha.H_l\left(\frac{\sqrt{2}(x-b)}{w_{ox}}\right).\exp\left(\frac{-(x-b)^2}{w_{0x}^2}\right).\exp\left(\frac{j\pi(x-b)^2}{\lambda R_{0x}}\right).H_m\left(\frac{\sqrt{2}y}{w_{0y}}\right).\exp\left(\frac{-y^2}{w_{0y}^2}\right).\exp\left(\frac{j\pi y^2}{\lambda R_{0y}}\right) \quad (2)$$

where w_{0x}= 2µm and w_{0y} = 2µm are the *x* and *y* spot sizes respectively, *b* is the radial offset from the core center; R_{0x}= 0 and R_{0y} = 0 are the *x* and *y* radii of curvature respectively; H_l and H_m are Hermite polynomials. The radial offset, *b*, is varied on the interval *b* = 1µm to 10µm for performance analysis. The VCSEL is connected to a vortex lens used to transform the flat phase front to a helical phase front. The focal length of lens, *f*=8. 0mm and the vortex order, *m* = 4.The applied phase transformation is expressed as [27]:

$$t(x,y)=\exp\left[-j\left(\frac{n\pi r^2}{2\lambda f}+m\theta\right)\right] \quad (3)$$

$$r=x^2+y^2 \quad (4)$$

$$\theta=\tan^{-1}(y/x) \quad (5)$$

where *x* and *y* are transverse coordinates in the *x*-*y* plane, λ is the signal wavelength, *m* is the vortex order, *n* is the material index and *f* is the lens focal length. Fig. 2 shows the amplitude and phase distributions of the transverse electric field of the

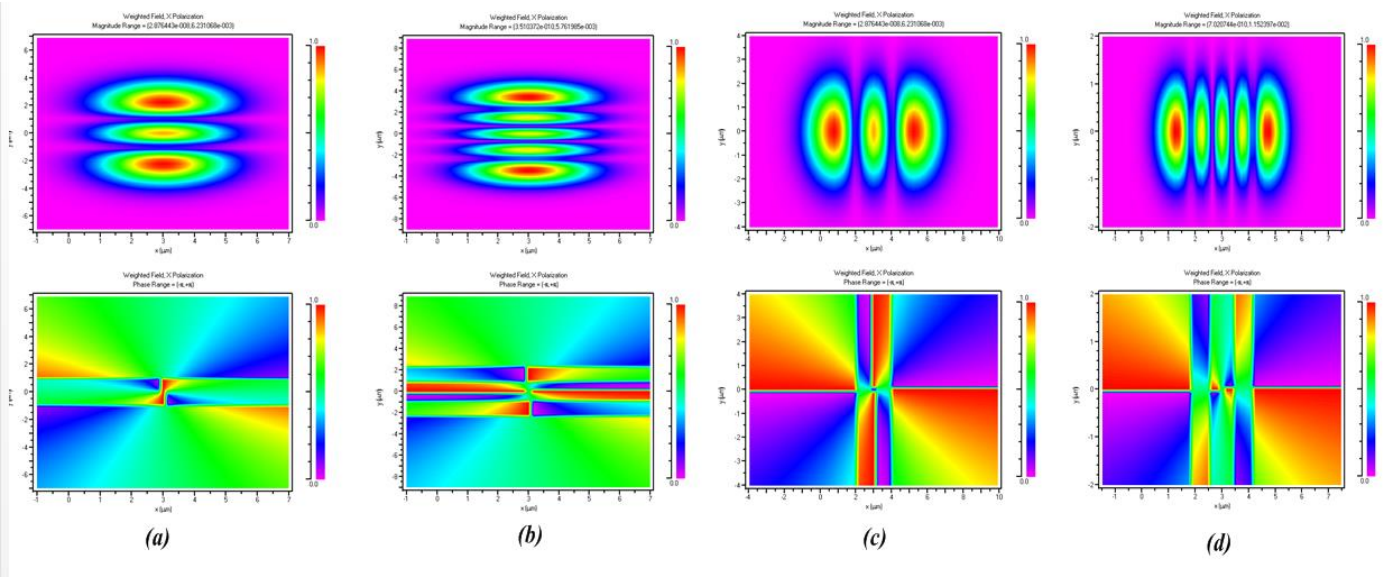

Fig. 3 Magnitude distribution (top) and phase distributions (bottom) of the transverse electric field of both helical-phased ring mode and HG mode from the VCSEL array, incident at the MMF input facet for different HG modes: (a) HG_{02} (b) HG_{04} (c) HG_{20} and (d) HG_{40}

generated ring mode after the vortex lens. Fig. 3 shows the magnitude and phase distributions of the transverse electric field of helical-phased HG mode of different *x*-indices and *y*-indices from the VCSEL array. Fig. 4 shows the magnitude and phase distributions of the transverse electric fields of both helical-phased ring mode and various HG mode from the VCSEL array after the vortex lens, incident at the MMF input facet.

The four independent MDM signals are then propagated through a 1500m-long manufactured MMF. The assumed value for attenuation is 1.5 dB/km with consideration of power modal coupling. The measured refractive index profile of the manufactured MMF is shown in Fig. 5.

Two photodetectors are used to retrieve the de-WDM-ed signals. The modes are then demultiplexed at the photodetectors based on a noninterferometric modal decomposition [4] to retrieve the four channels.

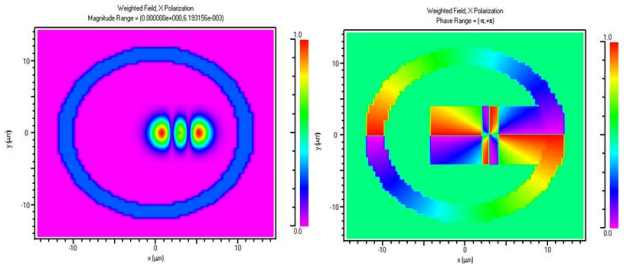

Fig. 4 magnitude (left) and phase distributions (right) of the transverse electric field of both helical-phased ring mode and HG mode after vortex lens

The power coupling coefficients, modal delays and BER performances are analyzed for different HG modes. The results and analyses are presented in Section III.

Results and Discussion

Fig. 6 shows the power coupling coefficients into MMF linearly polarized (LP) modes versus modal delay after for Channel 2 output. The impulse responses obtained from the new mode combination are narrower with the excitation of predominantly higher-ordered modes compared to the impulse pulses for the excitation of pure helical-phased HG modes [29]. For the investigation of radial offsets, it is observed that a radial offset, b of 3μm achieves the best impulse response. This is consistent with experimental results from MDM of HG modes [30, 31] where the optimal radial launch for alleviating modal dispersion and increasing bandwidth capacity in MMF is less than 3μm.

Fig. 7 illustrate the degenerate mode groups (DMG) and the relative group delays of the DMGs. From the curves, it is evident that the lowest DMD is achieved when for HG_{20}. Also, HG_{20} exhibits the best suppression of power into odd mode

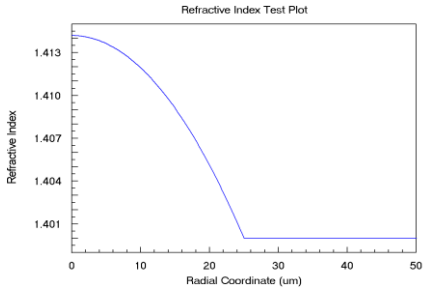

Fig. 5 Measured refractive index profile of manufactured MMF in MDM model

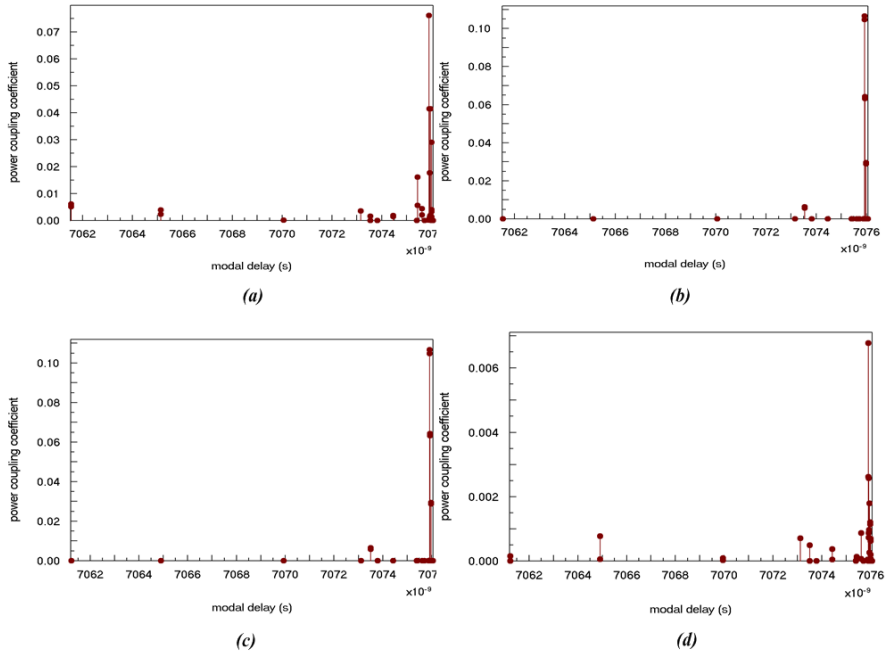

Fig. 6 Power coupling coefficients into LP modes versus modal delay at Channel 3 output for different HG modes at 1500 m: (a) HG_{02} (b) HG_{04} (c) HG_{20} and (d) HG_{40}

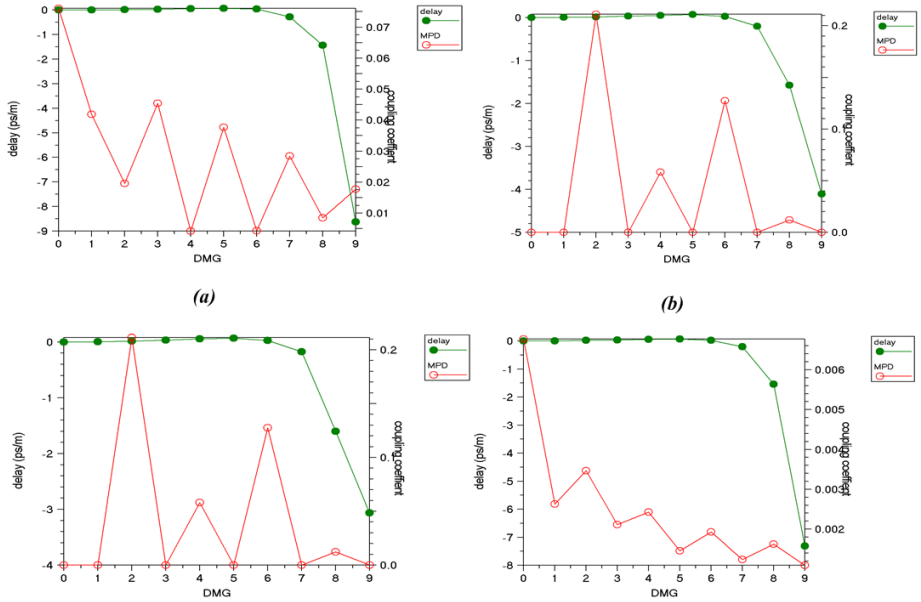

Fig. 7 Relative group delay versus DMG (green) and power coupling coefficient versus DMG (red) for Channel 3 output for different HG mode: (a) HG_{02} (b) HG_{04} (c) HG_{20} (d) HG_{40}

Fig. 7 shows the power coupling coefficients versus groups, resulting in a large contrast ratio between more dominant mode groups. This ensures that destructive interference between the propagating mode groups is constrained. Thus, HG_{20} is the most robust compared to HG_{02}, HG_{04} and HG_{40} although radial offset of twin anti-phase spots demonstrate better suppression of symmetric modes [32]

For a comparison of the different HG modes, the BER at Channel 3 were examined, as shown in Table 1. Consistent with the power coupling coefficients and modal delays in Fig. 6 and Fig. 7, the lowest BER is attained for HG_{20}, followed by HG_{04}, HG_{40}, and HG_{02}. The BER performance implies that the *y*-index change affects the channel more profoundly than the *x*-index of the Hermite polynomial.

In a typical data center, MMF lengths are mostly shorter than 500 meters [33]. The MMF link yield for the proposed MDM model is 1500m, thus satisfying the length requirement for data centers

Conclusion

A four-channel 44Gbps data transmission is achieved for MDM of a set of helical-phased center-launched ring modes and radially offset helical-phased HG modes on wavelengths 1550.12nm and 1551.72nm. The lowest BER is attained for HG_{20}, followed by HG_{04}, HG_{40}, and HG_{02} at a radial offset of 3µm. The MDM model could be viable for parallel optical interconnects in data centers.

References

[1] K. Nisar, A. Amphawan, and S. B. Hassan, "Comprehensive Structure of Novel Voice Priority Queue Scheduling System Model for VoIP Over WLANs," *Int. Journal of Advanced Pervasive and Ubiquitous Computing (IJAPUC)* vol. 3, pp. 50 – 70, 2011.

[2] R. Essiambre, G. Kramer, P. J. Winzer, G. J. Foschini, and B. Goebel, "Capacity Limits of Optical Fiber Networks," *J. Lightwave Tech*, 2010.

[3] D. Coleman, D. Kozichek, and C. Sparks. (2013) Optical Connectivity Trends in the Data Center: Migration from 10G to 40G to 100G with OM3/OM4 Multimode fiber *BICSI News*.

[4] A. Amphawan, "Holographic mode-selective launch for bandwidth enhancement in multimode fiber," *Optics Exp.*, vol. 19, pp. 9056-9065, 2011.

[5] A. Amphawan, "Binary encoded computer generated holograms for temporal phase shifting," *Optics Exp.*, vol. 19, pp. 23085-23096, 2011.

[6] A. Amphawan, "Binary spatial amplitude modulation of continuous transverse modal electric field using a single lens for mode selectivity in multimode fiber," *J. Mod. Opt.*, vol. 59, pp. 460-469, 2012.

[7] A. Amphawan and D. O'Brien, "Holographic Mode Field Generation for a Multimode Fiber Channel," in *IEEE Int. Conf. on Photon. 2010 (ICP2010)*, Langkawi, 2010, pp. 1-5.

[8] R. A. Panicker and J. M. Kahn, "Algorithms for compensation of multimode fiber dispersion using adaptive optics," *Journal of Lightwave Technology*, vol. 27, pp. 5790-5799, 2009.

[9] R. A. Panicker, A. P. T. Lau, J. P. Wilde, and J. M. Kahn, "Experimental comparison of adaptive optics algorithms in 10-Gb/s multimode fiber systems," *Journal of Lightwave Technology*, vol. 27, pp. 5783-5789, 2009.

[10] M. B. Shemirani, J. P. Wilde, and J. M. Kahn, "Adaptive compensation of multimode fiber dispersion by control of launched amplitude, phase, and polarization," *Journal of Lightwave Technology*, vol. 28, pp. 2627-2639, 2010.

[11] N. Bai, E. Ip, Y.-K. Huang, E. Mateo, F. Yaman, M.-J. Li, *et al.*, "Mode-division multiplexed transmission with inline few-mode fiber amplifier," *Optics Express*, vol. 20, pp. 2668-2680, 2012.

[12] E. Ip, M.-J. Li, Y.-K. Huang, A. Tanaka, E. Mateo, W. Wood, *et al.*, "146λx6x19-Gbaud wavelength-and mode-division multiplexed transmission over 10x50-km spans of few-mode fiber with a gain-equalized few-mode EDFA," in *Optical Fiber Communication Conference*, 2013, p. PDP5A. 2.

[13] C. Koebele, M. Salsi, D. Sperti, P. Tran, P. Brindel, H. Mardoyan, *et al.*, "Two mode transmission at 2x100Gb/s, over 40km-long prototype few-mode fiber, using LCOS-based programmable mode multiplexer and demultiplexer," *Optics Express*, vol. 19, pp. 16593-16600, 2011.

[14] R. Ryf, N. K. Fontaine, M. Montoliu, S. Randel, B. Ercan, H. Chen, *et al.*, "Photonic-Lantern-Based Mode Multiplexers for Few-Mode-Fiber Transmission," in *Optical Fiber Communication Conference*, 2014, p. W4J. 2.

[15] R. Ryf, S. Randel, N. K. Fontaine, M. Montoliu, E. Burrows, S. Chandrasekhar, *et al.*, "32-bit/s/Hz spectral efficiency WDM transmission over 177-km few-mode fiber," in *Optical Fiber Communication Conference*, 2013, p. PDP5A. 1.

[16] R. Ryf, S. Randel, A. H. Gnauck, C. Bolle, A. Sierra, S. Mumtaz, *et al.*, "Mode-division multiplexing over 96 km of few-mode fiber using coherent 6 6 MIMO processing," *Lightwave Technology, Journal of*, vol. 30, pp. 521-531, 2012.

[17] A. Amphawan, N. M. A. A. Samman, and B. Nedniyom, "Selective excitation of LP01 mode in multimode fiber using solid-core photonic crystal fiber," *J. Mod. Opt.*, vol. 60, 2013.

[18] T. Kaiser, D. Flamm, and M. DuparrÚ, "Complete modal decomposition for optical fibers using CGH-based correlation filters," *Optics express*, vol. 17, pp. 9347-9356, 2009.

[19] A. Amphawan and D. O'Brien, "Modal decomposition of output field for holographic mode field generation in a multimode fiber channel," in *Photonics (ICP), 2010 International Conference on*, 2010, pp. 1-5.

[20] Z. Jiang and J. R. Marciante, "Precise Modal Decomposition in Multimode Optical Fibers by Maximizing the Sum of Modal Power Weights," in *Frontiers in Optics*, 2008, p. FMD4.

[21] G. Milione, H. Huang, M. P. J. Lavery, T. A. Nguyen, G. Xie, Y. Cao, *et al.*, "Orbital-angular-momentum mode (de)multiplexer: A single optical element for MIMO-based and non-MIMO-based multimode fiber systems," in *Optical Fiber Communications Conf. and Exhibition (OFC)*, San Francisco, CA, 2014, pp. 1-3.

[22] A. N. Alexeyev, T. Fadeyeva, A. V. Volyar, and M. S. Soskin, "Optical vortices and the flow of their angular momentum in a multimode fiber," *Semiconductor Physics, Quantum Electronics and Optoelectronics*, vol. 1, pp. 82-89, 1998.

[23] N. Bozinovic, Y. Yue, Y. Ren, M. Tur, P. Kristensen, H. Huang, *et al.*, "Terabit-Scale Orbital Angular Momentum Mode Division Multiplexing in Fibers," *Science*, vol. 340, pp. 1545-1548, 2013.

[24] P. Boffi, P. Martelli, A. Gatto, and M. Martinelli, "Mode-division multiplexing in fibre-optic communications based on orbital angular momentum " *J. Opt* vol. 15, p. 075403, 2013.

[25] L. Z. Yan Yan, Jian Wang, Jeng-Yuan Yang, Irfan M. Fazal, Nisar Ahmed, Alan E. Willner and S. J. Dolinar, "Fiber structure to convert a Gaussian beam to higher-order optical orbital angular momentum modes," *Opt. Lett. 37*, vol. 37, pp. 3294-3296, 2012.

[26] B. A.V. and Y. K.A., "Research of refractive index profile defects of silica graded-index multimode fibers of telecommunication cables," *Infocomminication Technologies*, vol. 8, pp. 22-27, 2010.

[27] R. D. Group, "OptSim User Guide," 2010.

[28] X. Xue and A. G. Kirk, "Transverse modal characterization of VCSELs based on intensity measurement," in *Optoelectronic Interconnects VII; Photon. Packaging and Integration II,*, San Jose, CA, 2000, p. 144.

[29] A. Amphwan, Y. Fazea, R. Din, and M. N. Omar, "Effect of Vortex Order on Transmission of Spiral-Phased Donut Mode in Multimode Fiber," presented at the The 3rd International Conference on Internet Services Technology and Information Engineering (ISTIE 2015), Bali, Indonesia., 2015.

[30] L. Geng, S. H. Lee, K. Williams, R. Penty, I. White, and D. Cunningham, "Symmetrical 2-D hermite-gaussian square launch for high bit rate transmission in multimode fiber links," in *Optical Fiber Communication Conf.*, 2011, p. OWJ5.

[31] Y. Li, J. D. Ingham, V. Olle, G. Gorden, R. V. Penty, and I. White, "20 Gb/s Mode-Group-Division Multiplexing employing Hermite-Gaussian Launches over Worst-Case Multimode Fiber Links," in *Optical Fiber Communication Conf.*, 2014, pp. 1-3.

[32] V. K. Dehariya, S. K. Shrivastava, and R. Jain, "Clustering of image data set using k-means and fuzzy k-means algorithms," in *Computational Intelligence and Communication Networks (CICN), 2010 International Conference on*, 2010, pp. 386-391.

[33] Y. Benlachtar, R. Bouziane, R. I. Killey, C. R. Berger, P. Milder, R. Koutsoyannis, *et al.*, "Optical OFDM for the data center," in *Transparent Optical Networks (ICTON), 2010 12th Int. Conf. on*, 2010, pp. 1-4.